FEBS Letters 586 (2012) 2306–2312

journal homepage: www.FEBSLetters.org

Structural and SAXS analysis of the budding yeast SHU-complex proteins

Zhun She [a], Zeng-Qiang Gao [a], Ying Liu [a], Wen-Jia Wang [a], Guang-Feng Liu [a], Eleonora V. Shtykova [b], Jian-Hua Xu [a], Yu-Hui Dong [a,*]

[a] Beijing Synchrotron Radiation Facility, Institute of High Energy Physics, Chinese Academy of Sciences, Beijing 100049, China
[b] Institute of Crystallography, Russian Academy of Sciences, 59 Leninsky Pr., Moscow 117333, Russia

ARTICLE INFO

Article history:
Received 19 April 2012
Revised 8 June 2012
Accepted 14 June 2012
Available online 27 June 2012

Edited by Christian Griesinger

Keywords:
DNA repair
Protein-complex
Paralog
SAXS
DNA binding

ABSTRACT

In *Saccharomyces cerevisiae*, four proteins, Shu1, Shu2, Psy3 and Csm2, form a stable SHU-complex both in vivo and in vitro. These proteins are involved in the early stages of the homologous recombination DNA damage repair process. In this paper, the crystal structure of the Psy3–Csm2 sub-complex is presented at 1.8 Å resolution and successfully fitted into our small angle X-ray scattering (SAXS) data of the SHU-complex. Taken together with our electrophoretic mobility shift assay (EMSA) results, a model is proposed for the SHU–protein complex coupled with DNA.

Structured summary of protein interactions:
PSY3 and **CSM2** bind by X-ray crystallography (View interaction)
PSY3, **CSM2**, Shu 1 and **Shu 2** physically interact by x ray scattering (View interaction)

1. Introduction

The DNA repair mechanism is crucial for maintaining genomic stability in cells and mutations of DNA repair proteins can lead to cancer or cell death. A group of DNA-repair related proteins Psy3, Csm2, Shu1 and Shu2 was found in budding yeast, and these proteins form the stable SHU-complex. Mutations of SHU-complex proteins were first identified to suppress *SGS1* and *TOP3* methyl methanesulfonate (MMS) sensitivity [1,2], and the complete deletion of the four proteins did not show additional MMS sensitivity when compared with any of the single residue mutants [1]. Strong interactions between the four proteins have been found using a two-hybrid system [1,3], suggesting that the four proteins form a stable complex that functions in the same epistasis group [1,2,4,5].

The roles of the SHU-complex proteins were further investigated by mutagenesis with other homologous recombination repair (HRR) genes Rad51, RAD54 and Rmi1 [2,4]. A model was proposed that the yeast SHU-complex may play an important role in coupling error-free post-replication repair (PRR) to homologous recombination (HR) [4].

Further studies found that Shu1 functions with an anti-recombinase DNA protein Srs2 to interact with a ribosomal DNA (rDNA) regulating protein UAF30, and the interactions between Shu1 and Srs2 are not confined to rDNA regulation [6]. Thus, by regulating Srs2 activity, the SHU-complex shifts the balance of DNA repair toward Rad51 filament stabilization [6].

Homologs of the SHU proteins were found in *Schizosaccharomyces pombe* and humans [5,7]. Psy3 shares homology with Rdl1 in fission yeast and Rad51D in humans, the latter protein was reported to contain an N-ter ssDNA binding domain and a conserved ATPase motif [7,8]. Shu2 is homologous to the Sws1 protein found in fission yeast and humans [5]. All three proteins contain Zn-finger like SWIM domains that are considered to be important for protein–protein/DNA interactions [9]. Shu1has homology with fission yeast protein Rlp1 and human protein XRCC2. Interestingly, human Sws1, Rad51d and XRCC2 proteins were reported to form a complex that is important in facilitating Rad51 activity [7]. These conserved protein complexes could infer a new mechanism in the regulation of Rad51 family protein activities throughout eukaryotes.

While we were preparing this paper, an independent study published the crystal structure of the Psy3–Csm2 heterodimer [10]. The study also showed that Psy3 and Csm2 can bind DNA, and located the loops responsible for DNA binding through mutagenesis [10].

Here, the crystal structure of the Psy3–Csm2 complex together with SAXS data of the whole SHU-complex in vitro is presented. The structures of Psy3 and Csm2 resemble each other and both share the similar architecture with the ATP core domain of proteins that belong to the Rad51 family. By combining biochemical experiments and the SAXS data, a proposed model of the SHU-complex

* Corresponding author.
E-mail address: dongyh@ihep.ac.cn (Y.-H. Dong).

0014-5793/$36.00 © 2012 Federation of European Biochemical Societies. Published by Elsevier B.V. All rights reserved.
http://dx.doi.org/10.1016/j.febslet.2012.06.024

binding to DNA is presented, and this model should further aid our understanding of the mechanism of this protein complex.

2. Material and methods

2.1. Cloning and expression

The genes encoding Psy3 and Csm2 were cloned into the pCDF-Deut vector (Novagen), whereas the shu1 and shu2 genes were cloned into the pETDeut (Novagen) vector. The primers for each gene are listed in the Supplementary Table 1. The constructed plasmids containing different gene combinations were transformed or co-transformed into the Rosetta2 (DE3) strain (Novagen). Large cultures were induced at OD_{600} = 0.6 with a final concentration of 0.5 mM isopropyl β-D-1-thiogalactopyranoside (IPTG) and left to express at 291 K for 16 h.

2.2. Protein purification and crystallization

The cells containing the Psy3 and Csm2 proteins were suspended in a buffer containing 500 mM NaCl, 50 mM Tris–HCl pH 8.0, 2 mM beta-mercaptoethanol (βME) and 1 mM phenylmethylsulfonyl fluoride (PMSF). After sonication, the lysate was centrifuged at 13 000×*g* for 60 min. The supernatant was then loaded onto a 5 mL HiTrap (Ni^{2+}) chelating HP column (GE Healthcare) and washed with 25–100 mM imidazole. The protein was eluted with 300 mM imidazole, ultra-filtered and passed through a HiLoad 16/60 Superdex 200 pg column (GE Healthcare) equilibrated with a buffer consisting of 500 mM NaCl, 50 mM Tris–HCl pH 8.0 and 2 mM dithiothreitol (DTT). The single sharp peak containing the target protein was collected and ultra-filtered to 20–30 mg/ml. Other combinations of complexes were purified in the same way.

The Psy3–Csm2 complex crystallization screening was carried out at 293 K using the sitting-drop vapor-diffusion technique. The best crystals were obtained within three days under the condition of 100 mM Tris–HCl, pH 8.0, 10% ethanol and 10% 2-methyl-2,4-pentadiol (MPD). The selenomethionine (SeMet) derivative was purified and crystallized as described above.

2.3. Data collection, structure determination and refinement

Both wild type and Se-Met substituted multiple-wavelength anomalous dispersion (MAD) data sets were collected at 100 K on the station BL17U1 of the Shanghai Synchrotron Radiation Facility (SSRF). All data were processed using the program package HKL2000 [11] and collection statistics are summarized in Table 1. Selenium atoms were located by the program SOLVE [12] and the initial phases were used for automatic model building by the program RESOLVE [13], which produced interpretable electron density. The phases from RESOLVE were transferred into the program ARP/wARP [14] for further model building. This model was further built and refined against the native data at 1.8 Å resolution with the program PHENIX.refine [15] and COOT [16]. The qualities of the final models were checked with the program MolProbity [17]. Data collection and refinement statistics are given in Table 1. The program PyMOL (http://www.pymol.sourceforge.net/) was used to prepare structural figures.

2.4. EMSA of the SHU-complex

One micromolar of ssDNA and dsDNA substrates (Supplementary Table 2) were incubated with different concentrations of the SHU-complex and sub-complex proteins in a 10 μL system at 293 K for 25 min. The binding buffer for reactions contains

Table 1
Data collection and refinement statistics for Psy3–Csm2.

	Peak	Remote	Native
Data collection			
Wavelength (Å)	0.9791	0.9	0.9791
Space group	c2	c2	c2
Unit-cell parameters	a = 134.93 Å, b = 50.10 Å, c = 76.95 Å, β = 103.17°	a = 134.99 Å, b = 50.13 Å, c = 77.01 Å, β = 103.17°	a = 135.33 Å, b = 51.16 Å, c = 77.05 Å, β = 103.02°
Resolution (Å)[a]	2.20 (2.24–2.20)	2.20 (2.24–2.20)	1.76 (1.79–1.76)
Unique reflections	25 288 (1283)	25 680 (1260)	46 537 (2353)
Completeness (%)	99.5 (100)	99.3 (99.9)	90.4 (91.9)
Redundancy	4.8 (4.7)	4.9 (5.0)	3.6 (3.4)
Mean *I*/? (I)	40.72 (8.13)	42.34 (8.16)	38.93 (2.55)
Molecules in asymmetric unit	1	1	1
R_{merge} (%)	7.6 (33.0)	6.2 (29.7)	4.3 (54.2)
Refinement			
Resolution range (Å)	29.86–1.80		
R_{work}/R_{free} (%)	20.3/22.8		
Average B factor (Å^2)			
Main chain (A/B)	39.22/44.58		
Side chain (A/B)	46.07/50.26		
Waters	50.20		
Number of atoms			
Residues (A/B)	192/210		
Protein (A/B)	1542/1633		
Waters	162		
Ramachandran plot (%)			
Most favoured	97.2		
Allowed	2.8		
R.m.s. deviations			
Bond lengths (Å)	0.007		
Bond angles (°)	1.137		

[a] The values in parenthesis means those for the highest resolution shell.

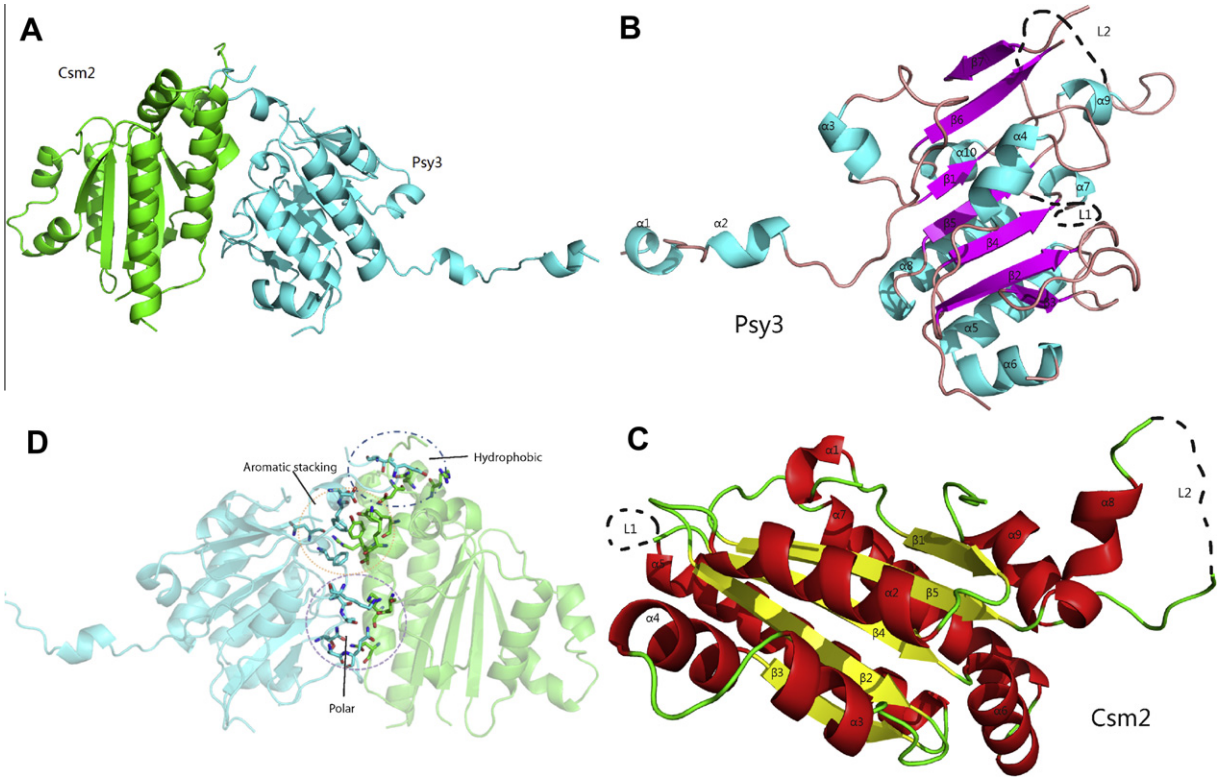

Fig. 1. Structure and interface of the Psy3–Csm2 heterodimer. (A) The overall structure of the Psy3–Csm2 complex. Psy3 is shown in cyan and Csm2 shown in green. (B, C) Secondary structures of Psy3 and Csm2. Missing loops in the electron density map are shown as hypothetical dashed lines. (D) The interface between Psy3 and Csm2.

20 mM Tris–HCl pH 8.0, 50 mM NaCl, 2 mM DTT, 4 mM $MgCl_2$ and 3% glycerol. After adding 2.5 μL loading buffer (50% glycerol, 0.02% bromophenol blue), the reaction mixtures were resolved in a native polyacrylamide gel in 1× TG buffer (25 mM Tris–HCl, 192 mM glycine, pH 8.3) at 277 K for 40–50 min and then visualized by ethidium bromide (EB) staining.

2.5. SAXS experiment and data analysis

The SHU-complex containing all four proteins was purified as described above and stored in the buffer containing 25 mM HEPES pH 7.0, 500 mM NaCl and 5 mM DTT. Synchrotron SAXS measurements were performed at the European Molecular Biology Laboratory (EMBL) on the storage ring DORIS III of the Deutsches Elektronen Synchrotron (DESY, Hamburg) on the X33 beamline [18] equipped with a robotic sample changer [19] and a PILATUS detector (DECTRIS, Switzerland). The scattering was recorded in the range of the momentum transfer $0.07 < s < 5.5\ nm^{-1}$, where $s = (4\pi\sin\theta)/\lambda$, 2θ is the scattering angle, and $\lambda = 0.15$ nm is the X-ray wavelength. The measurements were carried out in a vacuum cuvette with exposure times of 2 min to diminish the parasitic scattering. The experimental scattering profiles from the samples were corrected for background scattering by the solvent, and processed using standard procedures and the program PRIMUS [20]. The samples were measured at three different concentrations, 1.2, 2.5 and 5.0 mg/mL with further extrapolation to zero concentration. The latter was used for structural analysis. The distance distribution functions p(r) was computed using the program GNOM [21]. This function was used to determine a maximal size of the protein in solution and the output used for *ab initio* low resolution shape restoration by the programs DAMMIN [22] and GASBOR [23]. The low resolution envelope for a shape restored by the program DAMMIN was calculated by the program CRYSOL [24].

3. Results

3.1. The SHU-complex proteins in vitro

Our initial attempts to overexpress each protein of the SHU-complex in *Escherichia coli* and purify the proteins failed because the proteins were either expressed as inclusion bodies or aggregated when their fusion tags were removed in solution (data not shown). These observations strongly suggest that the four proteins depend on each other for their stability in vitro.

Various combinations were tried to test the interactions among the SHU-complex. Csm2 was not able to co-elute with Shu1 or Shu2 from a Ni^{2+} chelating column, which was in agreement with previous experiments [1,3]. The interaction between Psy3 and Shu2 was weak such that most of the co-expressed proteins were found in inclusion bodies when expressed together. Soluble purification of the two proteins together to sufficient levels was not possible. We managed to pull down the whole complex from a Ni^{2+} chelating column with only one Hex-his-tag at the N-terminus of Shu1 or Shu2, and the four proteins eluted as a single peak (Supplementary Fig. S1C) from a HiLoad 16/60 Superdex 200 pg column (GE Healthcare), indicating that their interactions in vitro are strong enough even in 500 mM NaCl. The SDS–PAGE electrophoresis results are shown in Supplementary Fig. S1A and B.

3.2. Crystal structure of the Psy3–Csm2 complex

The overall structure of the Psy3–Csm2 heterodimer is shown in Fig. 1A. Interestingly, although the Psy3 and Csm2 proteins share only a 17% sequence similarity, they resemble each other structurally. The general structures of the proteins are composed of a set of parallel β-sheets flanked by several α-helices. Our structures show that Psy3 contains ten helices and seven strands (Fig. 1B), whereas Csm2 contains nine helices and five strands (Fig. 1C).

The N-terminal part of Psy3 is largely composed of flexible loops, whereas the C-terminal region contains many regions where electron densities are missing. These parts may represent flexible regions that are important for protein–protein/DNA interactions, which we will discuss later. The structure of Csm2 is similar to that of Psy3, except for the N-terminal disordered region.

Psy3 and Csm2 interact with each other via various forces (Fig. 1D). Hydrogen bonds dominate the inter-protein interactions at the lower part of the interface, whereas hydrophobic interactions play an important part in maintaining the stability of the upper part, similar to the ball-and-socket module observed in the Rad51 polymerization motif [25]. The center of the protein–protein interface is stabilized by aromatic stacking.

3.3. Crystal structure comparisons

A structural similarity search was performed using the DALI 206 web server (http://ekhidna.biocenter.helsinki.fi/dali_server). Psy3 and Csm2 not only share similar architecture with each other (Fig. 2A), but both proteins also resemble the conserved ATP core domain of the Rad51 family recombinase.

Structural alignment of Psy3 and Csm2 with protein *Mycobacterium smegmatis* RecA (*Ms*RecA; PDB ID: 1UBC) returned RSMD values of 2.64 Å (144 Cα) and 2.60 Å (127 Cα), respectively. Fig. 2B shows the superposition of Csm2 with *Ms*RecA. The regions of the proteins that showed the highest superposition were found to be in the central parallel beta strands as well as the two longest helices (α5 and α8 for Psy3, and α5 and α7 for Csm2). Mutagenesis data of several consecutive basic residues in the L2 loops of Psy3 and Csm2 have revealed that this loop appears to be important for DNA binding [10]. Therefore, we performed a structural alignment of the Psy3–Csm2 heterodimer with a part of the *E. coli* RecA-DNA structure (*Ec*RecA; PDB ID: 3CMT) [26], and the Psy3–Csm2 hetero-dimer fitted into the *Ec*RecA homo-dimer with an RSMD of 2.61 Å (154 Cα) for Psy3 and a value of 3.48 Å (133Cα) for Csm2 (Fig. 2C). More importantly, the L2 loops of Psy3 and Csm2 were found to superpose quite well with the L2 loops of *Ec*RecA, which is responsible for DNA binding (Fig. 2D and E), suggesting a similar DNA binding manner for the Psy3–Csm2 complex.

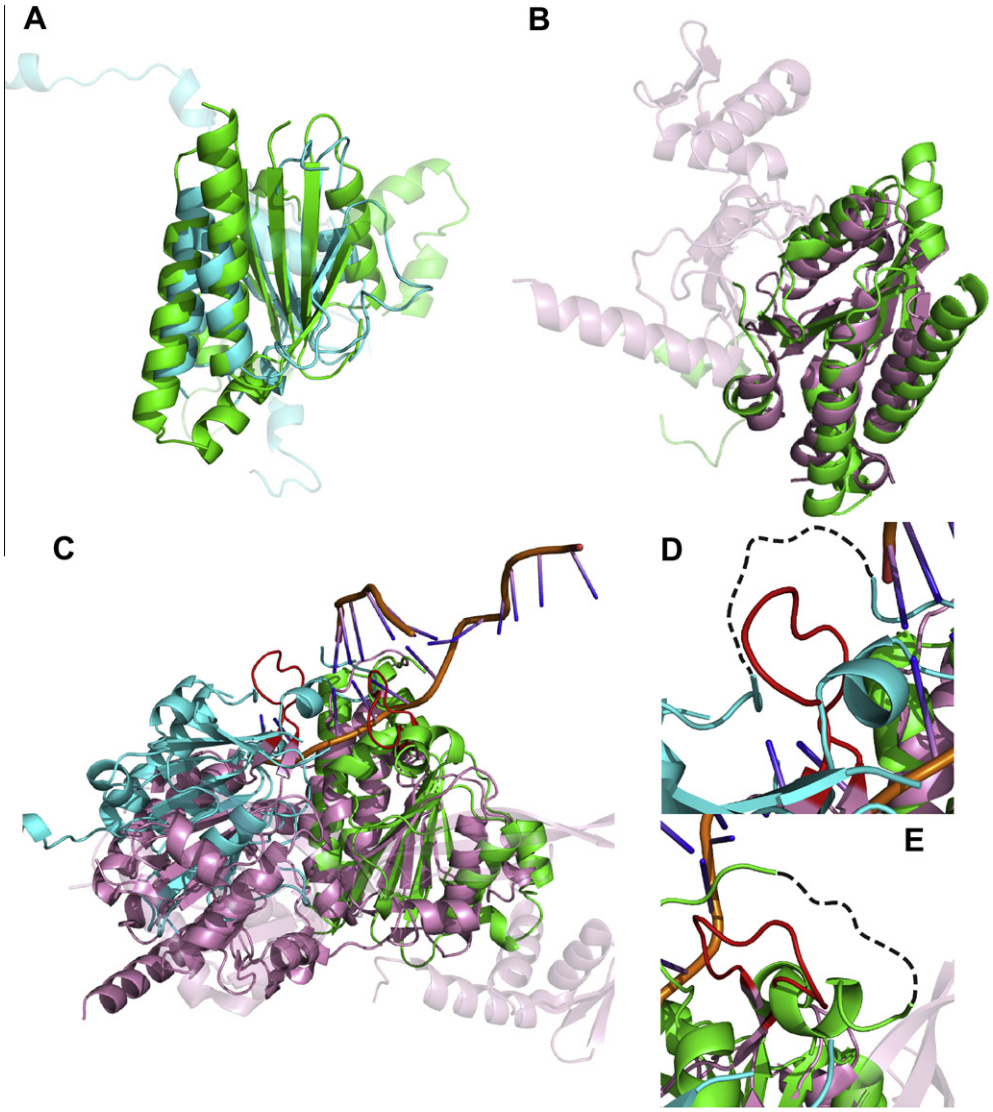

Fig. 2. Structural comparison among Psy3, Csm2 and Rad51 family proteins. (A) Superposition of Psy3 (cyan) with Csm2 (green). (B) Superposition of Csm2 (green) with *Ms*RecA (magenta). (C) Superposition of the Psy3 (cyan)–Csm2 (green) heterodimer with the *Ec*RecA homodimer (magenta)–DNA complex (L2 loops are colored in red). (D, E) Comparison of *Ec*RecA L2 loops (red) with Psy3 (cyan) and Csm2 (green) L2 loops (shown as hypothetical dashed lines).

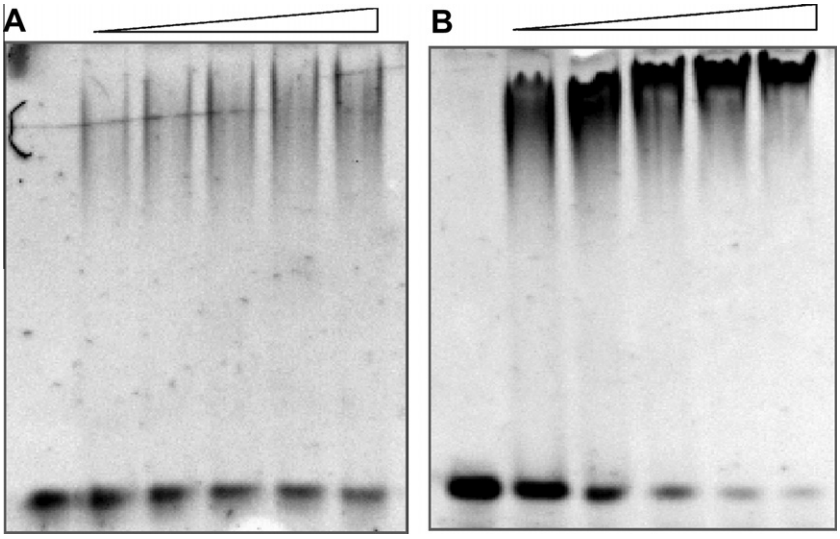

Fig. 3. EMSA results of the SHU-complex. (A) 1 μM ssDNA (36 nt) incubated with increasing amounts of the protein complex: 0, 1, 2, 3, 4 and 5 μM (lanes 1–6). (B) 1 μM dsDNA (29 bp) incubated with increasing amounts of the protein complex: 0, 1, 2, 3, 4 and 5 μM (lanes 1–6).

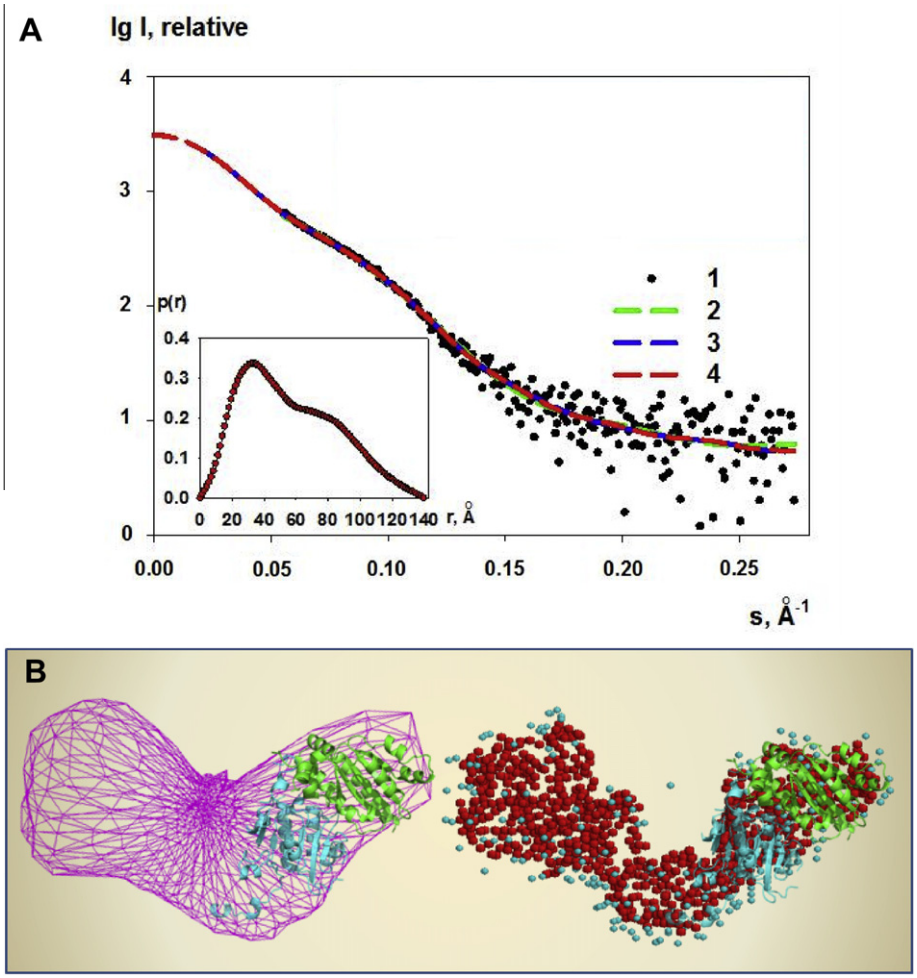

Fig. 4. SAXS curves and models. (A) Experimental scattering curve from the RSME protein in solution: 1 – experimental SAXS curve; 2 – scattering patterns computed from the DAMMIN model; 3 – scattering patterns computed from the GASBOR model; 4 – smooth curve back transformed from p(r) and extrapolated to zero scattering angle for the SHU-complex in solution. Inserts: left below – the distance distribution functions p(r) computed by the program GNOM for the SHU-complex in solution. (B) Low resolution structures of the RSME protein in solution with superposition of the Psy3–Csm2 crystal structure: left – envelope of the DAMMIN model; right – GASBOR model.

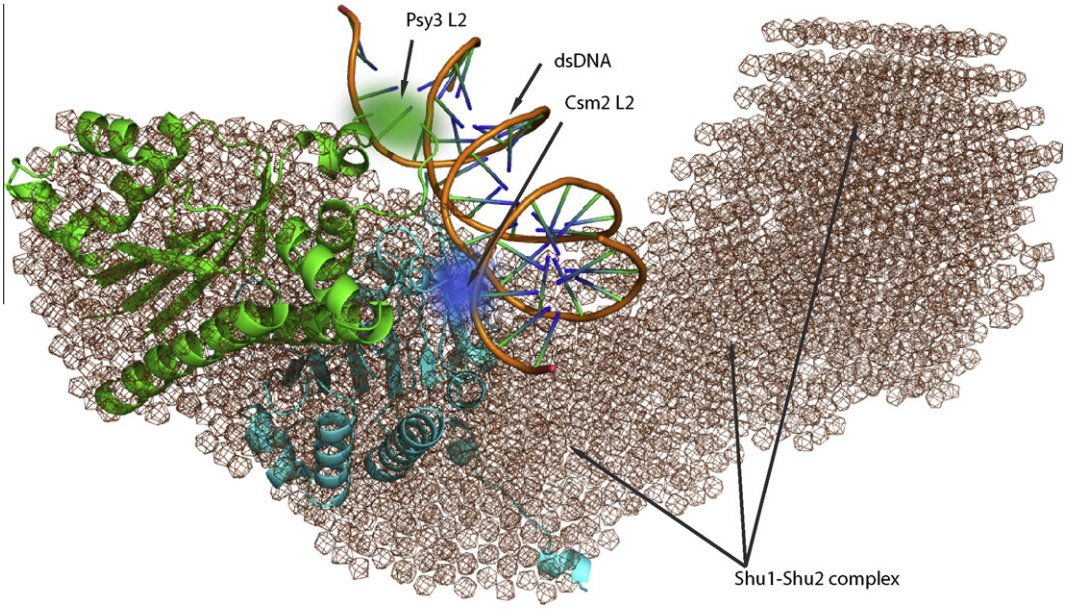

Fig. 5. The proposed model of the SHU-complex coupled with dsDNA in perspective view. The SHU-complex binds to one fragment of dsDNA (PDB ID: 1EA4). The SAXS DAMMIN model is presented using brown meshes, Psy3 is colored in cyan, whereas Csm2 is colored green. DNA goes across the groove of the SAXS model flanked by the two L2 loops of Psy3 and Csm2 (in blue and green shadows).

Additionally, the conserved walker B motif in Psy3, which is composed of the "GIVID" motif, and forms β4 of Psy3, is also very similar to other Rad51 family homologs. These important similarities in key functional motifs among Psy3–Csm2 and other Rad51 family proteins strongly suggest that the SHU-complex proteins are divergent homologs of the Rad51 family paralog proteins.

3.4. The SHU-complex binds to DNA

Our EMSA results have further proved that the SHU-complex possesses DNA binding ability. The Shu1–Shu2 complex alone did not show any ability to bind ssDNA or dsDNA, and EMSA of Psy3–Csm2, Psy3–Shu1 and Psy3–Csm2–Shu1 sub-complexes aggregated severely at a low salt concentration (data not shown). However, the complete SHU-complex was stable at a low salt concentration and possesses appreciable ability to bind DNA. Moreover, the SHU-complex showed greater affinity to bind dsDNA than ssDNA (Fig. 3A and B). After changing several DNA substrates, we also confirmed that the DNA binding ability of the SHU-complex showed no obvious sequence preferences (data not shown).

3.5. The conformation of SHU-complex in solution

Our SAXS data revealed the overall conformation of the SHU-complex in solution. Calculations using different models yielded similar profiles of the SHU proteins (Fig. 4A), and all model curves yielded very good fits to the experimental data with discrepancies of ~0.8.

The SHU-complex takes the shape of a boomerang, in which the structure of Psy3–Csm2 was successfully fitted into the right half of the envelope (Fig. 4B). Given that Csm2 does not interact with Shu1 and Shu2, it is very plausible that Csm2 locates on one edge of the complex. Psy3 lies in the center of the complex, connecting Shu1 and Shu2 mainly through its N-terminal loop, whereas the Shu1–Shu2 complex was positioned on the other half of the complex. The L2 loops of Psy3 and Csm2 locate close to the bottom of the concave. Together with our EMSA results, the structural data strongly indicates that DNA filaments may be attached to the bottom of the concave, making stable interactions with the SHU-complex.

4. Discussion

The Rad51 paralogs are a family of proteins that generally promote recombination DNA repair by facilitating the formation of Rad51 filaments in the early steps of HR. However, little was known about the specific mechanism of their functions until recently when a group discovered that a Rad51 paralog protein complex in budding yeast, Rad55–Rad57, mediates the formation of the Rad51 filaments by binding to Srs2 with Rad51 simultaneously [27]. Thus, it was suggested that the mechanism of Rad51 paralogs in promoting HR lies in the anti-antirecombination roles they play via their interaction with Srs2 and Rad51 family recombinases [27].

Many of the Rad51 paralog family of proteins possess certain degrees of DNA binding ability. However, these proteins appear to prefer different types of DNA substrates. The budding yeast Rad55–Rad57 complex binds ssDNA more strongly than dsDNA [28], whereas the human Rad51B-C-D-XRCC2 complex preferentially binds to branched DNA strands [29]. In this paper, we have discovered that the budding yeast SHU-complex showed greater affinity towards dsDNA than ssDNA. This suggests that the SHU-complex may play a complementary role to the Rad55–Rad57 complex in antagonizing Srs2 activity with different DNA substrates.

The Psy3 and Csm2 L2 loops, which locate near the C-terminal region of both proteins and close to each other, represent the DNA binding sites [10]. Taken together with our SAXS data, we propose that the concave part of the SHU-complex boomerang shaped model forms a good scaffold for DNA binding. Although the Shu1–Shu2 complex did not bind DNA, they may contribute to the stabilization of DNA binding.

A model including our SAXS model, dsDNA and the L2 loops of the crystal structure is shown in Fig. 5. Since mutations in any of the four proteins leads to a similar phenotype [1], we strongly suggest that the integrity of the SHU-complex architecture is crucial for its efficient function in DNA binding and other activities.

In summary, our structural and biochemical studies have provided valuable information in the understanding of the Rad51 paralog family proteins. The SAXS model of the SHU-complex provides new insights that describe how this complex functions.

5. PDB accession number

Atomic coordinates and structure factors of Psy3–Csm2 were deposited in the Protein Data Bank under the accession number 4EQ6.

Acknowledgments

We are grateful to the staff members of SSRF and DESY for sample test and data collection. This work was supported by the grants from the National Basic Research Program of China (2009CB918600) and National Natural Science Foundation of China (Grant numbers 31100531 and 10979005).

Appendix A. Supplementary data

Supplementary data associated with this article can be found, in the online version, at http://dx.doi.org/10.1016/j.febslet.2012.06.024.

References

[1] Shor, E., Weinstein, J. and Rothstein, R. (2005) A genetic screen for top3 suppressors in *Saccharomyces cerevisiae* identifies SHU1, SHU2, PSY3 and CSM2: four genes involved in error-free DNA repair. Genetics 169, 1275–1289.
[2] Mankouri, H.W., Ngo, H.P. and Hickson, I.D. (2007) Shu proteins promote the formation of homologous recombination intermediates that are processed by Sgs1-Rmi1-Top3. Mol. Biol. Cell 18, 4062–4073.
[3] Ito, T., Chiba, T., Ozawa, R., Yoshida, M., Hattori, M. and Sakaki, Y. (2001) A comprehensive two-hybrid analysis to explore the yeast protein interactome. Proc. Natl. Acad. Sci. U.S.A. 98, 4569–4574.
[4] Ball, L.G., Zhang, K., Cobb, J.A., Boone, C. and Xiao, W. (2009) The yeast Shu complex couples error-free post-replication repair to homologous recombination. Mol. Microbiol. 73, 89–102.
[5] Martin, V., Chahwan, C., Gao, H., Blais, V., Wohlschlegel, J., Yates 3rd, J.R., McGowan, C.H. and Russell, P. (2006) Sws1 is a conserved regulator of homologous recombination in eukaryotic cells. EMBO J. 25, 2564–2574.
[6] Bernstein, K.A., Reid, R.J., Sunjevaric, I., Demuth, K., Burgess, R.C. and Rothstein, R. (2011) The Shu complex, which contains Rad51 paralogues, promotes DNA repair through inhibition of the Srs2 anti-recombinase. Mol. Biol. Cell 22, 1599–1607.
[7] Braybrooke, J.P., Spink, K.G., Thacker, J. and Hickson, I.D. (2000) The RAD51 family member, RAD51L3, is a DNA-stimulated ATPase that forms a complex with XRCC2. J. Biol. Chem. 275, 29100–29106.
[8] Kim, Y.M. and Choi, B.S. (2011) Structural and functional characterization of the N-terminal domain of human Rad51D. Int. J. Biochem. Cell Biol. 43, 416–422.
[9] Makarova, K.S., Aravind, L. and Koonin, E.V. (2002) SWIM, a novel Zn-chelating domain present in bacteria, archaea and eukaryotes. Trends Biochem. Sci. 27, 384–386.
[10] Tao, Y., Li, X., Liu, Y., Ruan, J., Qi, S., Niu, L. and Teng, M. (2012) Structural analysis of Shu proteins reveals a DNA-binding role essential for resisting damage. J. Biol. Chem..
[11] Otwinowski, Z. and Minor, W. (1997) Processing of X-ray diffraction data collected in oscillation mode. Method Enzymol. 276, 307–326.
[12] Terwilliger, T.C. and Berendzen, J. (1999) Automated MAD and MIR structure solution. Acta Crystallogr. Sect. D Biol. Crystallogr. 55, 849–861.
[13] Terwilliger, T.C. (2003) Automated main-chain model building by template matching and iterative fragment extension. Acta Crystallogr. Sect. D Biol. Crystallogr. 59, 38–44.
[14] Langer, G., Cohen, S.X., Lamzin, V.S. and Perrakis, A. (2008) Automated macromolecular model building for X-ray crystallography using ARP/wARP version 7. Nat. Protocols 3, 1171–1179.
[15] Adams, P.D., Afonine, P.V., Bunkoczi, G., Chen, V.B., Davis, I.W., Echols, N., Headd, J.J., Hung, L.W., Kapral, G.J., Grosse-Kunstleve, R.W., McCoy, A.J., Moriarty, N.W., Oeffner, R., Read, R.J., Richardson, D.C., Richardson, J.S., Terwilliger, T.C. and Zwart, P.H. (2010) PHENIX: a comprehensive Python-based system for macromolecular structure solution. Acta Crystallogr. Sect. D Biol. Crystallogr. 66, 213–221.
[16] Emsley, P. and Cowtan, K. (2004) Coot: model-building tools for molecular graphics. Acta Crystallogr. Sect. D Biol. Crystallogr. 60, 2126–2132.
[17] Laskowski, R.A., Macarthur, M.W., Moss, D.S. and Thornton, J.M. (1993) Procheck – a program to check the stereochemical quality of protein structures. J. Appl. Crystallogr. 26, 283–291.
[18] Roessle, M.W., Klaering, R., Ristau, U., Robrahn, B., Jahn, D., Gehrmann, T., Konarev, P., Round, A., Fiedler, S., Hermes, C. and Svergun, D. (2007) Upgrade of the small-angle X-ray scattering beamline X33 at the European Molecular Biology Laboratory, Hamburg. J. Appl. Crystallogr. 40, S190–S194.
[19] Round, A.R., Franke, D., Moritz, S., Huchler, R., Fritsche, M., Malthan, D., Klaering, R., Svergun, D.I. and Roessle, M. (2008) Automated sample-changing robot for solution scattering experiments at the EMBL Hamburg SAXS station X33. J. Appl. Crystallogr. 41, 913–917.
[20] Konarev, P.V., Volkov, V.V., Sokolova, A.V., Koch, M.H.J. and Svergun, D.I. (2003) PRIMUS: a windows PC-based system for small-angle scattering data analysis. J. Appl. Crystallogr. 36, 1277–1282.
[21] Svergun, D.I. (1992) Determination of the regularization parameter in indirect-transform methods using perceptual criteria. J. Appl. Crystallogr. 25, 495–503.
[22] Svergun, D.I. (1999) Restoring low resolution structure of biological macromolecules from solution scattering using simulated annealing. Biophys. J. 76, 2879–2886.
[23] Svergun, D.I., Petoukhov, M.V. and Koch, M.H.J. (2001) Determination of domain structure of proteins from X-ray solution scattering. Biophys. J. 80, 2946–2953.
[24] Svergun, D., Barberato, C. and Koch, M.H.J. (1995) CRYSOL – a program to evaluate X-ray solution scattering of biological macromolecules from atomic coordinates. J. Appl. Crystallogr. 28, 768–773.
[25] Shin, D.S., Pellegrini, L., Daniels, D.S., Yelent, B., Craig, L., Bates, D., Yu, D.S., Shivji, M.K., Hitomi, C., Arvai, A.S., Volkmann, N., Tsuruta, H., Blundell, T.L., Venkitaraman, A.R. and Tainer, J.A. (2003) Full-length archaeal Rad51 structure and mutants: mechanisms for RAD51 assembly and control by BRCA2. EMBO J. 22, 4566–4576.
[26] Chen, Z., Yang, H. and Pavletich, N.P. (2008) Mechanism of homologous recombination from the RecA-ssDNA/dsDNA structures. Nature 453, 489–494.
[27] Liu, J., Renault, L., Veaute, X., Fabre, F., Stahlberg, H. and Heyer, W.D. (2011) Rad51 paralogues Rad55-Rad57 balance the antirecombinase Srs2 in Rad51 filament formation. Nature 479, 245–248.
[28] Sung, P. (1997) Yeast Rad55 and Rad57 proteins form a heterodimer that functions with replication protein A to promote DNA strand exchange by Rad51 recombinase. Genes Dev. 11, 1111–1121.
[29] Yokoyama, H., Sarai, N., Kagawa, W., Enomoto, R., Shibata, T., Kurumizaka, H. and Yokoyama, S. (2004) Preferential binding to branched DNA strands and strand-annealing activity of the human Rad51B, Rad51C, Rad51D and Xrcc2 protein complex. Nucleic Acids Res. 32, 2556–2565.